Indonesian Journal of Electrical Engineering and Computer Science
Vol. 35, No. 2, August 2024, pp. 673~682
ISSN: 2502-4752, DOI: 10.11591/ijeecs.v35.i2.pp673-682

Advanced control of double stage grid-tied three phase photovoltaic systems with shunt active power filter

Fatim-Zahra Zaghar[1], Zineb Hekss[2], Mohamed Rafi[3], Abderraouf Ridah[1], R'hma Adhiri[1]
[1]LIMAT Lab, Faculty of Sciences Ben M'sick, Hassan II University, Casablanca, Morocco
[2]ESE lab, ENSEM of Casablanca, Hassan II University, Casablanca, Morocco
[3]Industrial Engineering Lab, Mohammed VI International Academy of Civil Aviation, Casablanca, Morocco

Article Info

Article history:

Received Feb 25, 2024
Revised Mar 18, 2024
Accepted Mar 30, 2024

Keywords:

Backstepping
Hybrid automaton
MPPT
PV system
Shunt active power filter

ABSTRACT

This paper explores the challenges associated with the control of a two-stage three-phase electrical grid connected to a photovoltaic (PV) system. The objectives encompass: i) maximizing the available PV power, ii) controlling the DC-link voltage to a predetermined setpoint, and iii) considering that power quality has become an important measure in a distribution electrical network where different loads are connected, the third objective will mainly focus on ensuring power factor correction (PFC). To achieve these objectives, two loops of nonlinear controller are developed. In the outer loop, the duty cycle of a boost converter is controlled using a hybrid technique of backstepping technique and the perturb & observe (P&O) algorithm. In addition, the inner loop employs a hybrid automaton approach to tackle the challenges of a three-phase shunt active power filter (SAPF). The results have been verified through numerical simulation using MATLAB/Simulink power systems environment.

Corresponding Author:

Fatim-Zahra Zaghar
LIMAT Lab, Faculty of Sciences Ben M'sick, Hassan II University
BP 7955 Casablanca, Morocco
Email: fatimzahra.zaghar-etu@etu.univh2c.ma

1. INTRODUCTION

Boost converters, widely employed in power supplies, battery-operated devices, and renewable energy, particularly solar power. Indeed, they play a pivotal role in managing fluctuating DC voltages from solar panels [1]–[5]. Despite their inherent nonlinearity presenting control challenges, electrical engineering has advanced DC-DC converter regulation through methods like proportional, integral and derivative (PID), fuzzy logic, and fractional fuzzy PI controllers with PSO [6], [7]. Attempts with cascade proportional integrator and robust PID controllers showed limitations in terms of performance [8], [9], leading to exploration of alternatives like sliding mode control [10] and robust PID controllers to address stability issues and delayed responses in varying operating conditions [11].

Researchers have studied robust nonlinear controllers to manage complex photovoltaic (PV) systems. An inventive power boost converter used a switched-capacitor setup and a sliding mode controller to lower voltage stress and improve DC voltage gain [12]. In another approach [13], an adaptive robust fuzzy PI control was created, but it encountered computational issues that need more investigation. In addressing challenges with traditional methods for tracking the maximum power point. Effective intelligent strategies like backstepping techniques [14] and sliding mode backstepping controllers [15] have emerged to tackle issues such as irradiation distortion and load imbalance. Integral backstepping, applied to DC–DC Three-level boost converters, demonstrated superior regulator performance [16]. These approaches, notably integral backstepping, showcase exceptional responsiveness in power quality across diverse scenarios, such as islanded microgrids [17] and microgrid connected PV systems [18].

On the AC side, enhancements include an adaptive reference PI controller for inverters to boost overall system performance [19]. However, the integration of electronic loads in commercial and industrial sectors introduces power quality issues due to their nonlinear nature. Harmonic and reactive currents distort AC power, impacting the power factor correction (PFC) and waveform of voltage at the point of common coupling [20]. The phase shunt active power filter (SAPF) have shown dynamic performance in meeting harmonic standards, minimizing semiconductors for enhanced speed, and filtering capability. The controller designs for SAPF, often based on averaged nonlinear models, deploy lyapunov technique-based nonlinear control for power factor correction in reduced-part three-phase SAPF [21]. SAPF-connected photovoltaic systems are acknowledged for efficiently delivering real power to nonlinear loads, reducing dependence on the power grid [22]. The introduction of a novel hybrid automaton model for power electronics systems, facilitating the consideration of continuous and discrete evolutions. This study lies in the integration of an overall three-phase system, encompassing both boost and inverter converters. Using intelligent methods to enhance stability, response time, and achieve PFC. It aims to introduce a nonlinear controller for the proposed system, utilizing conventional backstepping for boost converter and applying a hybrid automaton approach for controlling a three-phase SAPF currents to their desired reference generated by the harmonic detection algorithm. This paper is outlined as follows: section 2, system description and modeling. Section 3 outlines the design of controllers, followed by section 4 which covers numerical simulations and finally a conclusion.

2. DESCRIPTION AND MODELING OF THE SYSTEM

The system circuit is represented in Figure 1, featuring a PV module connected to a boost converter and three-phase inverter. On the AC side, a three-phase grid is established using resistors and inductors (r_{gi}, L_{gi}; i=1,2,3). Furthermore, the nonlinear load incorporates a full bridge rectifier. The SAPF utilizes an IGBT-based three-leg split capacitor voltage inverter.

The three-phase power grid operates at 230 V and 50 Hz, with grid resistance (2 mΩ) and inductance (0.2 mH). The nonlinear load includes inductance (500 mH), resistance (15 Ω), and leakage inductance (5 mH). Moreover, the photovoltaic system combines 14 series modules and 17 parallel strings. In addition, the SAPF involves filter resistance (8 mΩ), inductance (3 mH), and capacitance (6 mF).

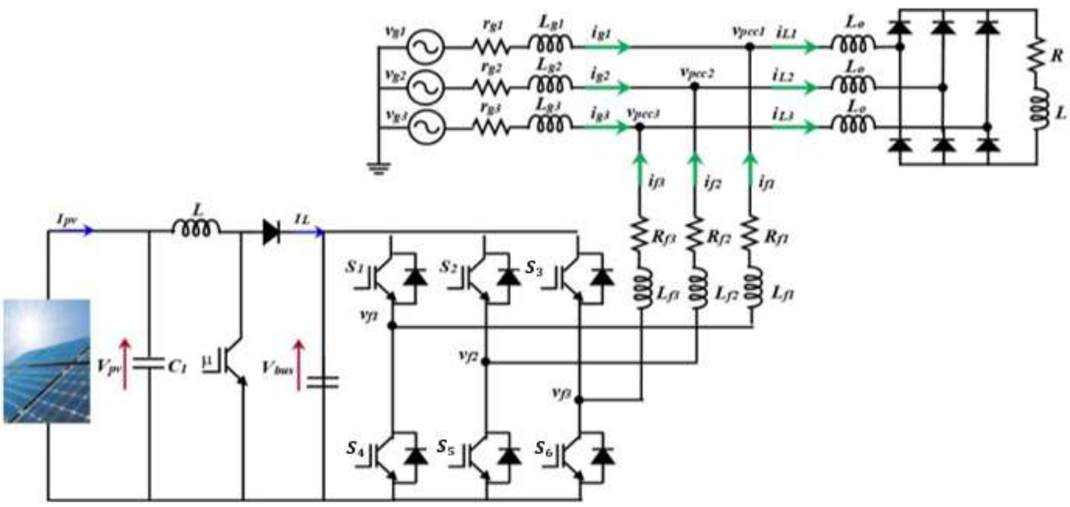

Figure 1. Diversity of controller applications in PV system

The voltages of the three-phase grid $\left(v_{gi}(t)\,;i=1,2,3\right)$ are expressed as follow:

$$v_{gi}(t)=E_g\sin\left(\omega_g t-\frac{2\pi}{3}(i-1)\right);i=1,2,3 \tag{1}$$

here, E_g represents the amplitude; ω_g signifies the angular frequency.

The currents' load ($i_{Lj}(t)$; $j = 1, 2, 3$) are then expressed through their Fourier expansion:

$$i_{Lj}(t) = \sum_{h=1}^{\infty} I_{L,h} \, sin(h(\omega_g t + \varphi_{j,h})) \; ; j = 1, 2, 3 \quad (2)$$

here, $I_{L,h}$ represents the amplitude, and ($\varphi_{j,h}$) signifies the harmonic current's phase with an order *h*.

2.1. Instantaneous model

The inverter's switching functions, μ_1, μ_2, and μ_3, are established in the following manner:

$$\mu_i = \begin{Bmatrix} 1 \; if \; S_{i1} \; is \; ON; \; S_{i2} \; is \; OFF \\ -1 \; if \; S_{i1} \; is \; OFF; \; S_{i2} \; is \; ON \end{Bmatrix} \quad (3)$$

utilizing Kirchhoff's laws, we formulated the following description:

$$L_g \frac{d}{dt}\begin{pmatrix} i_{g1} \\ i_{g2} \\ i_{g3} \end{pmatrix} = -r_g \begin{pmatrix} i_{g1} \\ i_{g2} \\ i_{g3} \end{pmatrix} + \begin{pmatrix} v_{g1} \\ v_{g2} \\ v_{g3} \end{pmatrix} - \begin{pmatrix} v_{pcc1} \\ v_{pcc2} \\ v_{pcc3} \end{pmatrix} \quad (4)$$

$$L_f \frac{d}{dt}\begin{pmatrix} i_{f1} \\ i_{f2} \\ i_{f3} \end{pmatrix} = -r_g \begin{pmatrix} i_{f1} \\ i_{f2} \\ i_{f3} \end{pmatrix} + \begin{pmatrix} v_{f1} \\ v_{f2} \\ v_{f3} \end{pmatrix} - \begin{pmatrix} v_{pcc1} \\ v_{pcc2} \\ v_{pcc3} \end{pmatrix} \quad (5)$$

$$L_f \frac{dV_{bus}}{dt} = i_{bus} \quad (6)$$

$$\begin{pmatrix} V_{f1} \\ V_{f2} \\ V_{f3} \end{pmatrix} = \frac{1}{2}\begin{pmatrix} 1 & 0 & 0 \\ 0 & 1 & 0 \\ 0 & 0 & 1 \end{pmatrix}\begin{pmatrix} \mu_1 \_1 \\ \mu_2 \_1 \\ \mu_3 \_1 \end{pmatrix}(V_{bus}) \quad (7)$$

2.2. Hybrid model of the inverter

The inverter's IGBT operates in eight distinct modes as presented in (8):

$$\dot{x} = f_{qi}(x) = A_{qi}x + B_{qi}; i = 1, \dots, 8 \quad (8)$$

the system's state is specified as:

$$x = [i_{f1}, i_{f2}, i_{f3}, v_{bus}]^T \quad (9)$$

3. CONTROLLERS DESIGN

A nonlinear hybrid method which consists of backstepping, and perturb & observe (P&O) is designed to control the boost converter. Additionally, a controller is established for the SAPF. It comprises two key parts: a harmonic detection method and hybrid automaton control.

3.1. Backstepping approach

The reference voltage is denoted as V_{-opt}. The error and its derivative can be expressed as follow [23]:

$$e_1 = V_{-opt} - V_{pv} \quad (10)$$

$$\dot{e}_1 = \dot{V}_{-opt} - \frac{I_{PV}}{C} + \frac{x_2}{C} \quad (11)$$

taking the Lyapunov function (12) and upon deriving the Lyapunov function (13), the results are as follow:

$$V_1 = \frac{1}{2}e_1^2 \quad (12)$$

$$\dot{V}_{-opt} - \frac{I_{PV}}{C} + \frac{x_2}{C} = -K_1 e_1 \quad (13)$$

to ensure system's stability, it is crucial to use the Lyapunov function, as cited in references [24], [25].

$$\dot{V}_1 = -k_1 {e_1}^2 \quad (14)$$

Second stage aims to track β reference current by establishing and error e_2 and its derivative:

$$e_2 = \beta - \frac{x_2}{C} \quad (15)$$

$$\dot{e}_2 = \dot{\beta} - \frac{V_{pv}}{L\,C} + \frac{V_{bus}}{L\,C}(1-\mu) \quad (16)$$

to ensure the convergence of both errors, a composite Lyapunov function (V_c) and its derivative are defined:

$$V_c = V_1 + \frac{1}{2}e_2^2 \quad (17)$$

$$\dot{V}_c = -k_1 {e_1}^2 + e_2\,\dot{e}_2 \quad (18)$$

then, $\dot{e}_2$ is considered as follows:

$$\dot{e}_2 = \dot{\beta} - \frac{V_{pv}}{L\,C} + \frac{V_{bus}}{L\,C}(1-\mu) - e_1 \quad (19)$$

finally, the following equation α is employed to stabilize the boost converter.

$$\mu = 1 - \left[\frac{L.C}{V_{bus}}\left(-K_2 e_2 + e_1 - \dot{\beta}\right) + \frac{V_{PV}}{V_{bus}}\right] \quad (20)$$

3.2. Harmonic detection algorithm

The study suggests using the synchronous detection algorithm as an efficient alternative to the instantaneous power theory for unbalanced three-phase grids. The unity signals can be calculated using expressions (18). While V_{g1}, V_{g2}, V_{g3} are the three-phase sinusoidal voltage:

$$u_{gi}(t) = \frac{V_{gi}}{V_{gm}}\ ;\ i=1,2,3 \quad (21)$$

the peak value of source voltages (V_{sm}) can be calculated as follows:

$$V_{gm} = [\tfrac{2}{3}(V_{g1}^2 + V_{g2}^2 + V_{g3}^2)]^{1/2} \quad (22)$$

the target peak of the reference source current (I_{gm}) involves two components and is calculated as follows:

$$I_{gm}^* = I_{gmp}^* + I_{gmd}^* \quad (23)$$

I_{smp}, is linked to the average load active power. Thus, we presume a distribution of the average load active power (p_{Lav}) among the three phases after compensating for reactive and harmonic currents.

$$p_g = \frac{3}{2} V_{gm} I_{gmp}^* = p_{Lav} \quad (24)$$

The fundamental component incorporates a second-order Butterworth low-pass filter is given by:

$$p_{Lav} = \frac{1}{T}\int_0^T p_L(t)\ ; T = \frac{1}{f} \quad (25)$$

within this context, p_{Lav} denotes the average value, while T corresponds to the period of the signal p_L.

$$p_L(t) = v_{ga} i_{La} + v_{gb} i_{Lb} + v_{gc} i_{Lb} \quad (26)$$

The instantaneous power of the load is denoted by p_L. Therefore, I_{gmp}^* can be carried out using (27):

$$I_{gmp}^{*} = \frac{2}{3}\frac{p_{Lav}}{Vgm} \tag{27}$$

considering the desired currents as follows:

$$i_{gi}^{*}(t) = I_{gm}^{*}.u_{gi} \text{ ; where i=1,2,3} \tag{28}$$

ultimately, the instantaneous reference currents for the active power filter (APF) are established as follows:

$$i_{refi}^{*}(t) = I_{gi}^{*} - i_{Li} \text{ ; where i=1,2,3} \tag{29}$$

3.3. Hybrid automaton control

The controllers' structure are described in Figure 2. The description of a hybrid automaton is encapsulated as follow:
H = {Q, X, F, N, E}; a finite set of discrete states $Q = \{q_i, i\epsilon(1, \ldots, 8)\}$, the continuous state space ($X = Ȓ^4$).
F: Q x X→ T^4 is the vector field linked with each discrete state.
E: N →2^X is the guard condition where E is the set of possible transitions.

The system involves the switching between 8 modes. The selection of each mode is determined by the conditions related to filter currents and their references.

$$\text{Mode 1 : (000)} =\{x\epsilon Ȓ^8 / I_{f1} < I_{fref1} \ and \ I_{f2} < I_{fref2} \ and \ I_{f3} < I_{fref3}\} \tag{30}$$

$$\text{Mode 2 : (001)} =\{x\epsilon Ȓ^8 / I_{f1} < I_{fref1} \ and \ I_{f2} < I_{fref2} \ and \ I_{f3} > I_{fref3}\} \tag{31}$$

$$\text{Mode 3 : (010)} =\{x\epsilon Ȓ^8 / I_{f1} < I_{fref1} \ and \ I_{f2} > I_{fref2} \ and \ I_{f3} < I_{fref3}\} \tag{32}$$

$$\text{Mode 4 : (011)} =\{x\epsilon Ȓ^8 / I_{f1} < I_{fref1} \ and \ I_{f2} > I_{fref2} \ and \ I_{f3} > I_{fref3}\} \tag{33}$$

$$\text{Mode 5 : (100)} =\{x\epsilon Ȓ^8 / I_{f1} > I_{fref1} \ and \ I_{f2} < I_{fref2} \ and \ I_{f3} < I_{fref3}\} \tag{34}$$

$$\text{Mode 6 : (101)} =\{x\epsilon Ȓ^8 / I_{f1} > I_{fref1} \ and \ I_{f2} < I_{fref2} \ and \ I_{f3} > I_{fref3}\} \tag{35}$$

$$\text{Mode 7 : (110)} =\{x\epsilon Ȓ^8 / I_{f1} > I_{fref1} \ and \ I_{f2} > I_{fref2} \ and \ I_{f3} < I_{fref3}\} \tag{36}$$

$$\text{Mode 8 : (111)} =\{x\epsilon Ȓ^8 / I_{f1} > I_{fref1} \ and \ I_{f2} > I_{fref2} \ and \ I_{f3} > I_{fref3}\} \tag{37}$$

The set of potential transitions, denoted as E(R_{ij}) = E(q_i, q_j); (j=i=l, ...,8), is given by:

$$E(R_{21}) = E(R_{31}) + E(R_{41}) + E(R_{51}) + E(R_{61}) + E(R_{71}) = E(R_{81}) = I_{f1} < I_{fref1} \ and \ I_{f2} < I_{fref2} \ and \ I_{f3} < I_{fref3} \tag{38}$$

$$E(R_{12}) = E(R_{32}) + E(R_{42}) + E(R_{52}) + E(R_{62}) + E(R_{72}) = E(R_{82}) = I_{f1} < I_{fref1} \ and \ I_{f2} < I_{fref2} \ and \ I_{f3} > I_{fref3} \tag{39}$$

$$E(R_{13}) = E(R_{23}) + E(R_{43}) + E(R_{53}) + E(R_{63}) + E(R_{73}) = E(R_{83}) = I_{f1} < I_{fref1} \ and \ I_{f2} > I_{fref2} \ and \ I_{f3} < I_{fref3} \tag{40}$$

$$E(R_{14}) = E(R_{24}) + E(R_{34}) + E(R_{54}) + E(R_{64}) + E(R_{74}) = E(R_{84}) = I_{f1} < I_{fref1} \ and \ I_{f2} > I_{fref2} \ and \ I_{f3} > I_{fref3} \tag{41}$$

$$E(R_{15}) = E(R_{25}) + E(R_{35}) + E(R_{45}) + E(R_{65}) + E(R_{75}) = E(R_{85}) = I_{f1} > I_{fref1} \ and \ I_{f2} < I_{fref2} \ and \ I_{f3} < I_{fref3} \tag{42}$$

$$E(R_{16}) = E(R_{26}) + E(R_{36}) + E(R_{46}) + E(R_{56}) + E(R_{76}) = E(R_{86}) = I_{f1} > I_{fref1} \ and \ I_{f2} < I_{fref2} \ and \ I_{f3} > I_{fref3} \tag{43}$$

$$E(R_{17}) = E(R_{27}) + E(R_{37}) + E(R_{47}) + E(R_{57}) + E(R_{67}) = E(R_{87}) = I_{f1} > I_{fref1} \ and \ I_{f2} > I_{fref2} \ and \ I_{f3} < I_{fref3} \tag{44}$$

$$E(R_{18}) = E(R_{28}) + E(R_{38}) + E(R_{48}) + E(R_{58}) + E(R_{68}) = E(R_{78}) = I_{f1} > I_{fref1} \ and \ I_{f2} > I_{fref2} \ and \ I_{f3} > I_{fref3} \tag{45}$$

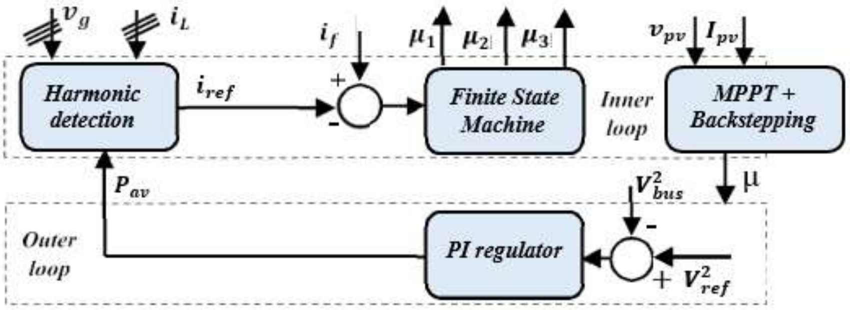

Figure 2. Controller structure of inner and outer loop

4. DISCUSSION AND RESULTS

The simulation investigates variations in solar irradiation and temperature as shown in Figures 3 and 4. In Figure 5, the hybrid backstepping technique with the P&O algorithm demonstrates dynamic performance, responding to an input voltage perturbation from 340 V to 400 V and stabilizing by 3.9s. Backstepping exhibits efficiency in diverse scenarios, showcasing strong tracking capabilities and rapid recovery.

Figure 6 illustrates an increase in real power extracted from photovoltaic panels between 0.5s and 2s, corresponding to the irradiation profile. The P_{mpp} curve closely aligns with the irradiation curve, indicating excellent MPPT performance. On the AC side, Figure 7 depicts harmonics in the filter current, rising with the I_{pv} behavior as shown in Figure 8. The grid current has a sinusoidal waveform with decreased magnitude as shown in Figure 9. While I_{pv} magnitude increases and demonstrating PFC achievement and THD as shown in Figures 10 and 11. Figure 12 shows the complete injection of maximum power from photovoltaic panels into the nonlinear load. Finally, Figure 13 reveals a three-phase control system utilizing a PI mechanism to regulate the DC bus voltage effectively, ensuring alignment with the desired reference level. The parameters used for PI are (K_P= 0.151, K_I= $5e^{-9}$).

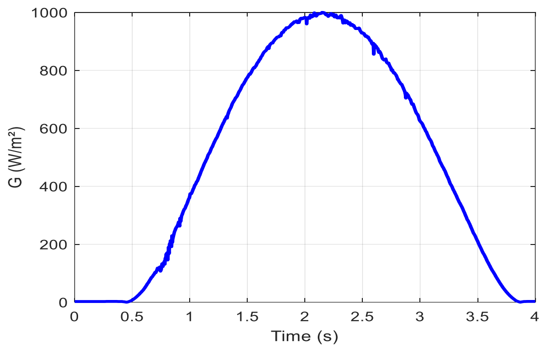

Figure 3. Solar irradiation profile

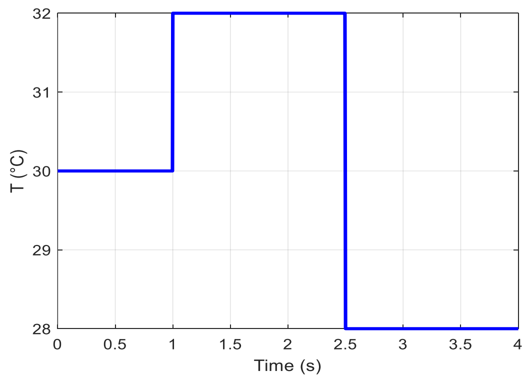

Figure 4. Temperature profile

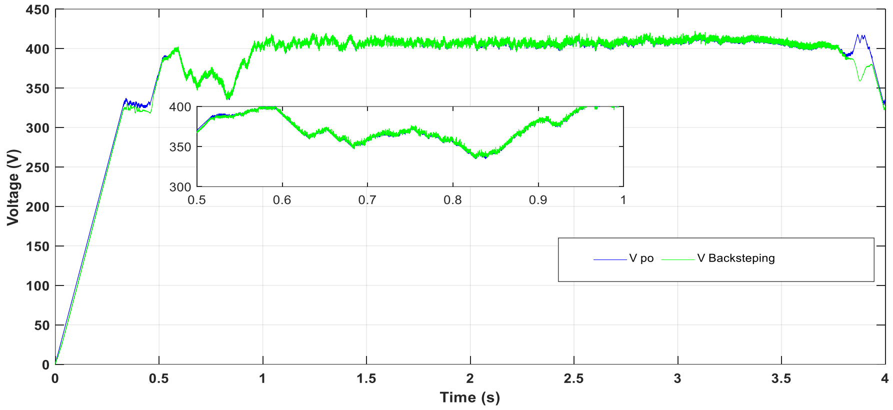

Figure 5. V_{bus} by applying backstepping

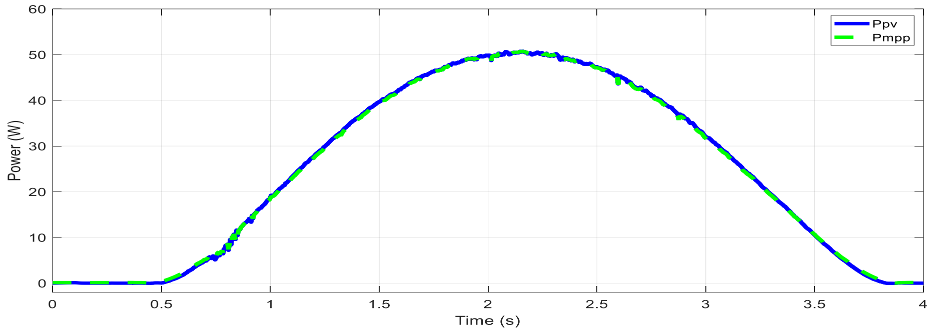

Figure 6. P_{mpp} and P_{pv} graphs

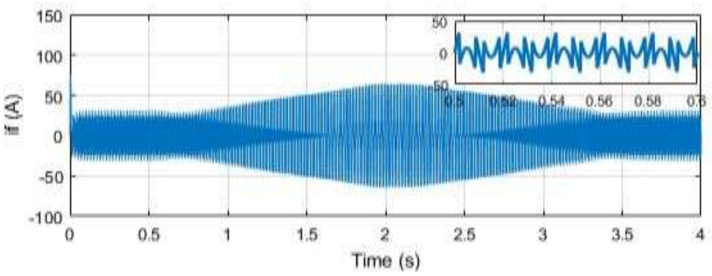

Figure 7. Filter current If

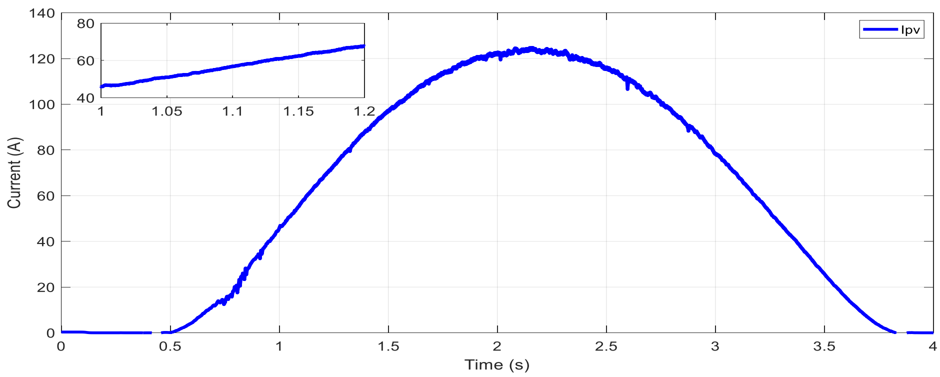

Figure 8. I_{pv} Behaviour graph

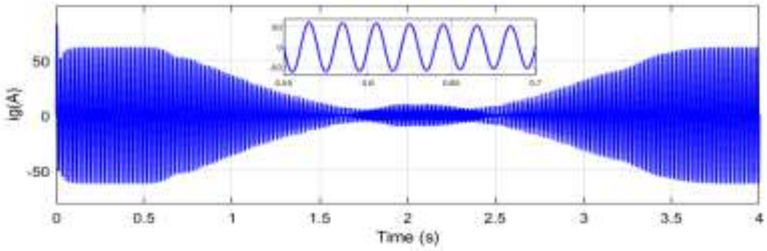

Figure 9. Grid current Ig

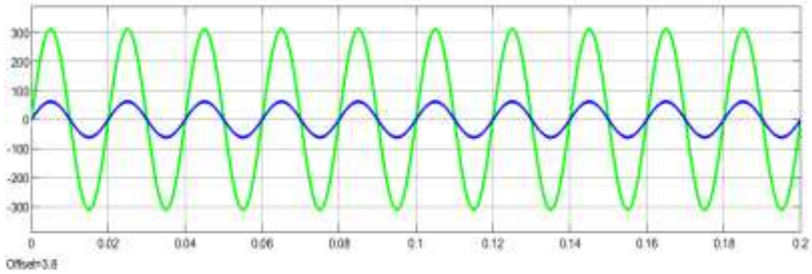

Figure 10. Unity power factor

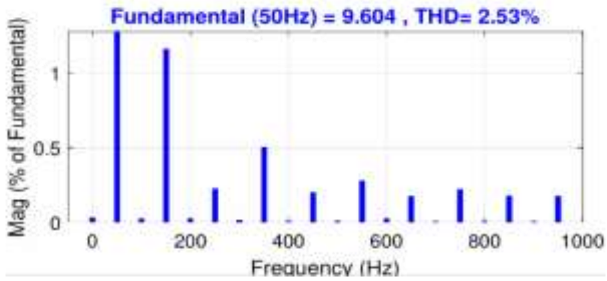

Figure 11. THD

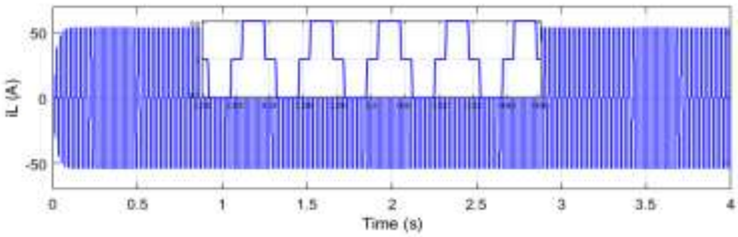

Figure 12. Load current I_L

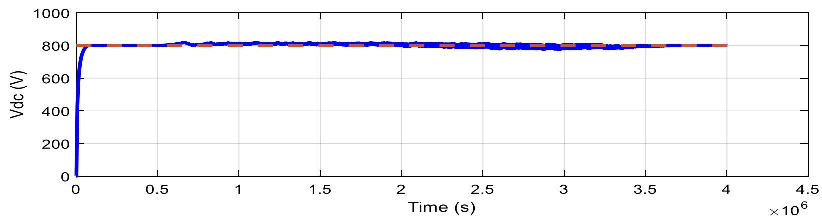

Figure 13. DC link voltage regulation

5. CONCLUSION

The research focuses on controlling a photovoltaic system connected to an electrical grid with a double-stage configuration in three phases. A nonlinear controller, employing backstepping technique, is designed to ensure system stability. The outer loop effectively addresses steady-state errors in DC bus voltage caused by mismatch interference, input voltage changes, and model uncertainty. Dynamic performance is obtained through Lyapunov stability conditions. A novel hybrid automaton approach is introduced for designing a controller for a three-phase SAPF linked to a photovoltaic system and nonlinear load, showing improved performance across various operating conditions. The study formally establishes the achievement of control objectives; extracting the maximum power from the PV system, including regulating DC-link voltage and achieving PFC.

REFERENCES

[1] H. S, J. R. A, B. G, and I. K, "Design and investigation of PV string/central architecture for bayesian fusion technique using grey wolf optimization and flower pollination optimized algorithm," *Energy Conversion and Management*, vol. 286, p. 117078, Jun. 2023, doi: 10.1016/j.enconman.2023.117078.

[2] A. Hayat, D. Sibtain, A. F. Murtaza, S. Shahzad, M. S. Jajja, and H. Kilic, "Design and analysis of input capacitor in DC–DC boost converter for photovoltaic-based systems," *Sustainability (Switzerland)*, vol. 15, no. 7, p. 6321, Apr. 2023, doi: 10.3390/su15076321.

[3] S. N. Rao, S. K. Anisetty, B. M. Manjunatha, B. M. K. Kumar, V. P. Kumar, and S. Pranupa, "Interleaved high-gain boost converter powered by solar energy using hybrid-based MPP tracking technique," *Clean Energy*, vol. 6, no. 3, pp. 460–475, Jun. 2022, doi: 10.1093/ce/zkac026.

[4] S. Chen *et al.*, "Research on topology of the high step-up boost converter with coupled inductor," *IEEE Transactions on Power Electronics*, vol. 34, no. 11, pp. 10733–10745, Nov. 2019, doi: 10.1109/TPEL.2019.2897871.

[5] M. Villegas-Ruvalcaba, K. J. Gurubel-Tun, and A. Coronado-Mendoza, "Robust inverse optimal control for a boost converter," *Energies*, vol. 14, no. 9, p. 2507, Apr. 2021, doi: 10.3390/en14092507.

[6] A. Rajavel and N. Rathina Prabha, "Fuzzy logic controller-based boost and buck-boost converter for maximum power point tracking in solar system," *Transactions of the Institute of Measurement and Control*, vol. 43, no. 4, pp. 945–957, Sep. 2021, doi: 10.1177/0142331220938211.

[7] M. Demirtas and F. Ahmad, "Fractional fuzzy PI controller using particle swarm optimization to improve power factor by boost converter," *International Journal of Optimization and Control: Theories and Applications*, vol. 13, no. 2, pp. 205–213, Jul. 2023, doi: 10.11121/ijocta.2023.1260.

[8] C. Yanarates and Z. Zhou, "Design and cascade PI controller-based robust model reference adaptive control of DC-DC boost converter," *IEEE Access*, vol. 10, pp. 44909–44922, 2022, doi: 10.1109/ACCESS.2022.3169591.

[9] T. Kobaku, R. Jeyasenthil, S. Sahoo, and T. Dragicevic, "Experimental verification of robust PID controller under feedforward framework for a nonminimum phase DC-DC boost converter," *IEEE Journal of Emerging and Selected Topics in Power Electronics*, vol. 9, no. 3, pp. 3373–3383, Jun. 2021, doi: 10.1109/JESTPE.2020.2999649.

[10] J. Rivera, S. Ortega-Cisneros, J. C. Rosas-Caro, and O. F. Ruíz-Martínez, "Sliding mode regulation of a boost circuit for DC-biased sinusoidal power conversion," *Applied Sciences (Switzerland)*, vol. 13, no. 10, p. 5963, May 2023, doi: 10.3390/app13105963.

[11] T. Kobaku, R. Jeyasenthil, S. Sahoo, R. Ramchand, and T. Dragicevic, "Quantitative feedback design-based robust PID control of voltage mode controlled DC-DC boost converter," *IEEE Transactions on Circuits and Systems II: Express Briefs*, vol. 68, no. 1, pp. 286–290, Jan. 2021, doi: 10.1109/TCSII.2020.2988319.

[12] Q. Qi, D. Ghaderi, and J. M. Guerrero, "Sliding mode controller-based switched-capacitor-based high DC gain and low voltage stress DC-DC boost converter for photovoltaic applications," *International Journal of Electrical Power and Energy Systems*, vol. 125, p. 106496, Feb. 2021, doi: 10.1016/j.ijepes.2020.106496.

[13] V. Kumar, A. Mitra, O. Shaklya, S. Sharma, and K. P. S. Rana, "An adaptive robust fuzzy PI controller for maximum power point tracking of photovoltaic system," *Optik*, vol. 259, p. 168942, Jun. 2022, doi: 10.1016/j.ijleo.2022.168942.

[14] M. Moutchou and A. Jbari, "Fast photovoltaic IncCond-MPPT and backstepping control, using DC-DC boost converter," *International Journal of Electrical and Computer Engineering*, vol. 10, no. 1, pp. 1101–1112, Feb. 2020, doi: 10.11591/ijece.v10i1.pp1101-1112.

[15] R. N. Deo, A. Shrivastava, and K. Chatterjee, "Implementation of sliding mode backstepping controller for boost converter in real-time for LED application," *Expert Systems*, vol. 40, no. 6, Jul. 2023, doi: 10.1111/exsy.13095.

[16] I. A. Ayad *et al.*, "Optimized nonlinear integral backstepping controller for DC-DC three-level boost converters," *IEEE Access*, vol. 11, pp. 49794–49805, 2023, doi: 10.1109/ACCESS.2023.3274773.

[17] A. A. Shah, X. Han, H. Armghan, and A. A. Almani, "A nonlinear integral backstepping controller to regulate the voltage and frequency of an islanded microgrid inverter," *Electronics (Switzerland)*, vol. 10, no. 6, pp. 1–24, Mar. 2021, doi: 10.3390/electronics10060660.

[18] N. Debdouche, L. Zarour, H. Benbouhenni, F. Mehazzem, and B. Deffaf, "Robust integral backstepping control microgrid connected photovoltaic system with battery energy storage through multi-functional voltage source inverter using direct power control SVM strategies," *Energy Reports*, vol. 10, pp. 565–580, Nov. 2023, doi: 10.1016/j.egyr.2023.07.012.

[19] A. Alhejji and M. I. Mosaad, "Performance enhancement of grid-connected PV systems using adaptive reference PI controller," *Ain Shams Engineering Journal*, vol. 12, no. 1, pp. 541–554, Mar. 2021, doi: 10.1016/j.asej.2020.08.006.

[20] S. Echalih, A. Abouloifa, I. Lachkar, Z. Hekss, M. Aourir, and F. Giri, "Hybrid control of single phase shunt active power filter based on interleaved buck converter," in *Proceedings of the American Control Conference*, Jul. 2019, vol. 2019-July, pp. 3636–3641, doi: 10.23919/acc.2019.8814917.

[21] Y. Abouelmahjoub, F. Giri, A. Abouloifa, F. Z. Chaoui, and M. Kissaoui, "Adaptive nonlinear control of reduced-part three-phase shunt active power filters," *Asian Journal of Control*, vol. 20, no. 5, pp. 1720–1733, Oct. 2018, doi: 10.1002/asjc.1681.

[22] Z. Hekss *et al.*, "Hybrid automaton control of three phase reduced switch shunt active power filter connected photovoltaic system," *IFAC-PapersOnLine*, vol. 53, no. 2, pp. 12847–12852, 2020, doi: 10.1016/j.ifacol.2020.12.1986.

[23] O. Diouri, N. Es-Sbai, F. Errahimi, A. Gaga, and C. Alaoui, "Modeling and design of single-phase PV inverter with MPPT algorithm applied to the boost converter using back-stepping control in standalone mode," *International Journal of Photoenergy*, vol. 2019, pp. 1–16, Nov. 2019, doi: 10.1155/2019/7021578.

[24] F. Z. Zaghar, E. M. Karami, M. Rafi, and A. Ridah, "Nonlinear backstepping control for photovoltaic system connected to the grid through inverter," in *Lecture Notes in Networks and Systems*, vol. 393, Springer International Publishing, 2022, pp. 315–326.
[25] S. Khadija, E. M. Ouadia, and F. Abdelmajid, "Nonlinear backstepping control of a partially shaded photovoltaic storage system," *Indonesian Journal of Electrical Engineering and Computer Science*, vol. 29, no. 1, pp. 225–237, Jan. 2023, doi: 10.11591/ijeecs.v29.i1.pp225-237.

BIOGRAPHIES OF AUTHORS

Fatim-Zahra Zaghar received an engineering degree in electrical engineering, electronics and telecommunication from Mohamed VI international academy of civil aviation Casablanca in 2017. She is currently pursuing the Ph,D. degree in physics and applications ate faculty of sciences Ben M'sik, Hassan II University of Casablanca. My research interests revolve around renewable energy systems, application of nonlinear control techniques to boost converters, and enhancing power quality in electrical energy. She can be contacted at email: fatizaghar@gmail.com.

Zineb Hekss received a master's degree in data processing from the Faculty of Sciences Ben M'sick, Hassan II University of Casablanca, in 2017, and the Ph.D. degree in Electrical Engineering and automatic control from the National Higher School of Electricity and Mechanics (ENSEM), Hassan II University of Casablanca, Morocco, in 2022. She is currently a Professor at Moroccan school of engineering. Her research interests include renewable energy systems, power quality. She can be contacted at email: zineb.hekss-etu@etu.univh2c.ma.

Dr. Mohamed Rafi is currently a Professor of engineering sciences in general and materials physics and applications of renewable energies in particular at the Mohammed VI International Academy of Civil Aviation. He has expertise in the performance of photovoltaic systems. In addition, his expertise is highly sought after in the case of ternary and quaternary materials used in thin layers such as a photovoltaic absorber and He is interested in modeling, design, prediction, and simulation problems of smart grid. He obtained His PhD in Materials Science and Engineering and his HDR in Renewable Energy. He can be contacted at: rafi3mhd@gmail.com.

Abderraouf Ridah Full Professor at University of Hassan II, Casablanca, Morocco. Skills and expertise: Renewable Energy, Photovoltaics, Solar Cells, Thin Films Technology and Nanotechnology, Material Characterization, Thin Film Deposition Materials, Semiconductor Device Physics, Electrical and optical Characterization, Solar Energy Materials, Electrical Conductivity, Film Technology, Optoelectronics, Ferroelectrics, Ferroelectric Materials, Phase Transitions Spectrum, Analytical Studies. He can be contacted at: abderraoufridah@yahoo.fr.

R'hma Adhiri is currently a full professor at Hassan II University, Faculty of Sciences Ben M'Sik, Department of Physics, in Casablanca, Morocco. Its main research activities are in the field of engineering sciences in general and materials physics in particular including photovoltaics and solar cells, electrical conductivity, dielectric materials. She can be contacted at: rahmadhiri@gmail.com.